

# Journal of Materials Chemistry B

Accepted Manuscript



This is an *Accepted Manuscript*, which has been through the Royal Society of Chemistry peer review process and has been accepted for publication.

*Accepted Manuscripts* are published online shortly after acceptance, before technical editing, formatting and proof reading. Using this free service, authors can make their results available to the community, in citable form, before we publish the edited article. We will replace this *Accepted Manuscript* with the edited and formatted *Advance Article* as soon as it is available.

You can find more information about *Accepted Manuscripts* in the [Information for Authors](#).

Please note that technical editing may introduce minor changes to the text and/or graphics, which may alter content. The journal's standard [Terms & Conditions](#) and the [Ethical guidelines](#) still apply. In no event shall the Royal Society of Chemistry be held responsible for any errors or omissions in this *Accepted Manuscript* or any consequences arising from the use of any information it contains.

Cite this: DOI: 10.1039/c0xx00000x

www.rsc.org/xxxxxx

PAPER

# Gold nanorod-seeded synthesis of Au@Ag/Au nanospheres with broad and intense near-infrared absorption for photothermal cancer therapy†

Xiaosheng Ye, Hui Shi,‡ Xiaoxiao He, Kemin Wang,\* Duo Li and Pengchao Qiu

Received (in XXX, XXX) Xth XXXXXXXXXX 20XX, Accepted Xth XXXXXXXXXX 20XX

DOI: 10.1039/b000000x

As a widely-adopted agent for photothermal therapy (PTT), gold nanorods (Au NRs) remain problematic due to the cytotoxicity derived from CTAB and the comparatively weak and narrow near-infrared (NIR) absorption band. To address this problem, we here proposed a shape-controllable and spectrum-adjustable synthesis method of Au@Ag/Au nanoparticles (NPs) through the first coating of a Ag nanolayer outside the Au NR seed and the subsequent replacement reaction with HAuCl<sub>4</sub> to yield a Ag/Au alloy nanoshell. Results from TEM and UV-vis spectra analysis showed that thicknesses of Ag layers directly determined NPs' shapes and sizes, and the formation of Ag/Au nanoshells effectively enhanced NPs' NIR absorbance. Remarkably, the optimum Au@Ag/Au nanospheres (NSs) with a diameter of ~40 nm were revealed to have a broad and intense absorption cross section from 400 to 1100 nm, ~4.7 times higher hyperthermia effect than Au NRs, and low dark-cytotoxicity. By using A549 lung cancer as the model, a series of *in vitro* investigations were performed and demonstrated that Au@Ag/Au NSs could efficaciously destruct cancer cells under a 980 nm irradiation. The PTT efficacy could be further improved by increasing NSs concentration, incubation time or irradiation time. Moreover, a preliminary *in vivo* study also showed that after injection into the A549 tumor, Au@Ag/Au NSs could cause an obvious necrosis at the irradiation site. It is indicated that a novel kind of promising and highly-effective NIR PTT agent has been developed, which might greatly advance the application of PTT in biomedical researches.

## 1 Introduction

As a promising alternative or supplement to conventional cancer treating approaches, photothermal therapy (PTT) has drawn considerable attention due to its advantages including minimal invasion, few complications, and fast recovery.<sup>1,2</sup> Typically, PTT utilizes optical absorbing agents to convert photons into local heating, thus promoting irreversible cancer destruction *via* protein denaturation and cell membrane disruption.<sup>3</sup> Its efficacy was greatly dependent upon optical absorbing properties of the adopted agents. Therefore, besides good biocompatibility and cancer-homing ability, ideal PTT agents are particularly desired to hold strong absorbance and efficient light-to-heat conversion in the near-infrared (NIR) region, where tissue transmissivity is highest as a result of low scattering and absorption from intrinsic chromophores.<sup>4,5</sup>

In recent years, development of nanotechnology has advanced the exploration of nanomaterials-based PTT agents. With varying degrees of success, a variety of NIR absorbing nanomaterials have been engineered and applied for photothermal ablation, such as gold nanorods (Au NRs),<sup>6-8</sup> gold nanocages,<sup>9,10</sup> gold nanoshells,<sup>11,12</sup> graphene oxide,<sup>13,14</sup> carbon nanotubes,<sup>15,16</sup> composite metal nanoparticles (NPs),<sup>17,18</sup> and so on. Thereinto, Au NRs, a kind of elongated NPs with one transverse and one longitudinal surface plasmon resonance (SPR) bands,<sup>19,20</sup> are of

particular interest. Owing to their superior properties including facile synthesis, flexible bioconjugation, colloidal stability and especially finely-tunable absorption range and large extinction coefficient in the NIR region, Au NRs have been extensively investigated for both *in vitro* and *in vivo* remote selective PTT of cancer.<sup>21-24</sup> However, concerning their future clinical uses, there are some deficiencies needed to be addressed. For instance, the further biomedical application of Au NRs might be limited by their cytotoxicity derived from the remaining excess cetyltrimethylammonium bromide (CTAB), which is a surfactant used as the template during preparation.<sup>25</sup> Although some ligand exchange methods have been developed to remove CTAB,<sup>25,26</sup> the additional exchange process might make the use of Au NRs complex and troublesome. Moreover, the absorbance intensity and light-to-heat conversion efficiency of Au NRs in the NIR region are also in need of improvement. In particular, the lack of a broad absorption cross section might hamper their popularity as widely adapted PTT agents, because it is inconvenient that the peak absorbance always have to be adjusted to match lasers with different irradiation wavelengths for optimum PTT effects.<sup>27-29</sup> Yeh *et al.* have reported a Au NR-in-shell nanostructure synthesis strategy by introducing Ag component and galvanic replacement reaction.<sup>30</sup> Basing on this strategy, rod-like PTT nanoagents with a broad absorption band were prepared and their spectrum could be further adjusted by controlling the gap size between core and shell.<sup>31</sup> However, in this strategy, bothersome multiple washing

steps were inevitable. More importantly, the preparation of Au NR-in-shell nanostructures with different shapes and the shape-induced spectrum variation has not been studied yet.

Herein, a simple, washing-free, shape-controllable and spectrum-adjustable synthesis method of Au@Ag/Au NPs has been proposed to develop a novel kind of PTT agent with a broad and strong NIR absorption cross section, highly efficient hyperthermia and low dark-cytotoxicity. Firstly, by coating Ag layers with different thicknesses and shapes outside Au NR seeds and then reacting with HAuCl<sub>4</sub> to yield Ag/Au alloy shells, a series of Au@Ag/Au NPs with different morphologies were synthesized. After investigating the effect of NPs' shapes on their optical and photothermal properties, the optimized Au@Ag/Au nanospheres (NSs) for NIR PTT were identified. Subsequently, a systematic study of Au@Ag/Au NSs for photothermal ablation of cancer cells was carried out with a 980 nm laser as the irradiation source. And on this basis, their efficacy for *in vivo* NIR PTT was also preliminarily valued.

## 2 Experimental

### 2.1 Chemicals and materials

Sodium borohydride (>96%) and silver nitrate (≥99.8%) were obtained from Sinopharm Chemical Reagent Co., Ltd. (Shanghai, China). Bovine serum albumin (BSA), polyvinyl pyrrolidone (PVP), cetyltrimethylammonium bromide (CTAB) and ascorbic acid were purchased from Dingguo Biotech. Co., Ltd. (Beijing, China). Calcein-AM and HAuCl<sub>4</sub>·H<sub>2</sub>O (>99.5%) were obtained from Sigma-Aldrich. All other reagents were of the highest grade available. Deionized water was prepared through the Nanopure Infinity™ ultrapure water system (Barnstead/Thermolyne Corp.).

### 2.2 Synthesis of Au NRs

Au NRs were prepared according to a room-temperature seedless growth method.<sup>19</sup> Firstly, 85 μL HAuCl<sub>4</sub> (40 mg/mL) and 5 mL CTAB (0.4 M) were mixed with 2.695 mL water. Then, 2 mL AgNO<sub>3</sub> (1 mM) and 200 μL ascorbic acid (100 mM) were added and stirred softly. Finally, 30 μL of NaBH<sub>4</sub> (1 mM) was rapidly mixed and the color of the solution changed to deep violet within a few minutes.

### 2.3 Synthesis of Au@Ag NPs

Au@Ag NPs with different shapes were synthesized using a washing-free and modified method.<sup>30</sup> Briefly, 510 μL of as-prepared Au NRs without washing were directly mixed with 10 mL 1 wt% of PVP, different volume of AgNO<sub>3</sub> (1 mM) and 250 μL of ascorbic acid (100 mM), followed by a gentle stir. When 0.5 mL of 0.1 M NaOH was added, the solution colour immediately started to change, implying the formation of Ag layer.

### 2.4 Synthesis of Au@Ag/Au NPs

Under a vigorously stir at 100 °C, 1.5 mL of HAuCl<sub>4</sub> (1 mM) was directly added to the as-prepared Au@Ag NPs without washing. The mixture was allowed to react for 15 min to produce Au@Ag/Au NPs. For biological applications, NPs were centrifuged and washed with saturated NaCl solution and distilled water.

### 2.5 Characterization of NPs

UV-vis spectral analysis was carried out using a Beckman Couiter DU800 spectrophotometer. The shape, size and element components of the as-prepared NPs were analyzed by high-resolution transmission electron microscopy (HRTEM, JEOL-3010) and energy-dispersive spectroscopy (EDS, Tecnai G2 F20 S-TWIN) at the accelerating voltage of 200 kV. Zeta potentials were determined in ultrapure water with a Malvern Zetasizer 3000 HS (Malvern, Worcestershire, England). Temperature elevation was induced by an external 0~18 W adjustable laser (980 nm, Beijing Hi-Tech Optoelectronic Co., China) as the irradiation source.

### 2.6 Cells

A549 cells (human lung adenocarcinoma cell line), SPCAi cells (human lung adenocarcinoma cell line) and QBC-939 cells (human cholangiocarcinoma cell line) were provided by the Cell Center of our lab. Cells were cultured in RPMI 1640 medium containing 10% fetal bovine serum, 100 μg/mL streptomycin and 100 IU/mL penicillin, and incubated at 37 °C in a humidified incubator containing 5% CO<sub>2</sub>.

### 2.7 Dark-cytotoxicity test

A549 cells were seeded in 24-well plates and allowed to grow overnight. After incubation with different concentrations of Au@Ag/Au NSs (0, 1.1×10<sup>10</sup>, 2.2×10<sup>10</sup>, 3.6×10<sup>10</sup>, 5.4×10<sup>10</sup>, and 1.1×10<sup>11</sup> particles/mL, respectively) at 37 °C for 6 h, cells were rinsed twice with PBS and then incubated in culture medium at 37 °C for 3 h. Finally, cell viability was tested using a propidium iodide (PI)-based dead cell staining method. Detailedly, cells were harvested and stained with PI (2 μM) for 15 min. Then, the dead cell percentage was analyzed using a FACSCalibur flow cytometer (BD Bioscience, USA).

### 2.8 Dark-field imaging

A549 cells seeded in cell culture dishes and allowed to grow overnight were firstly incubated with Au@Ag/Au NSs (2.2×10<sup>10</sup> particles/mL) for 6 h at 37 °C. Then, the cells were rinsed twice with PBS to remove excess NPs and fixed with 4% formaldehyde for 15 min at 37 °C. Finally, the interaction of Au@Ag/Au NSs and A549 cells were imaged using a dark-field microscope (Nikon Eclipse 80i) equipped with a black/white CCD camera.

### 2.9 *In vitro* NIR PTT

Cells seeded in 24-well plates and allowed to grow overnight were firstly incubated with NPs (2.2×10<sup>10</sup> particles/mL) for 6 h at 37 °C. Then, the cells were rinsed twice with PBS and received an irradiation from an external 980 nm laser. After gently rinsed with PBS, the cells were incubated in culture medium for 3 h at 37 °C. Finally, viability tests were performed by adding calcein-AM solution (0.6 μM) to stain living cells for 45 min. Fluorescent images were acquired using an inverted microscope (Nikon, Te300) with 4× objective lens. The effect of different conditions on PTT efficacies was systematically investigated, including NPs types, NSs concentrations, incubation time of NSs and cells, and irradiation time.

### 2.10 Animals

Male athymic BALB/c (Balb/C-nu) mice were purchased from the Shanghai SLAC Laboratory Animal Co., Ltd (BALB/c). All animal operations were in strict accordance with the Regulations for the Management of Laboratory Animals of the Ministry of Science and Technology of the People's Republic of China. The protocol was approved by the Committee on the Ethics of Animal Experiments of Hunan Provincial Laboratory Animal Center [Permit Number: SYXK (Xiang) 2008-0001]. Tumor-bearing animal models were prepared through a subcutaneous injection of  $\sim 10^6$  *in vitro*-propagated A549 cells into the backside of nude mice. Tumors were then allowed to grow to 1-2 cm in diameter for 2-3 months.

### 2.11 *In vivo* NIR PTT

A549 tumor-bearing mice firstly received an intratumoral injection of 50  $\mu$ L Au@Ag/Au NSs ( $2.2 \times 10^{10}$  particles/mL), and then were exposed to a NIR laser irradiation (980 nm) for 5 min at 26.5 mW. The PTT effect was monitored every day using an IVIS Lumina II *in vivo* imaging system (Caliper LifeScience, USA). Control groups include tumor-bearing mice without any treatments, tumor-bearing mice with only irradiation and tumor-bearing mice with only injection of Au@Ag/Au NSs.

## 3 Results and discussion

### 3.1 Synthesis and characterization of Au@Ag NPs

In order to enhance the PTT efficacy of Au nanorods (NRs), silver with greater thermal conductivity than gold was firstly introduced by coating a Ag layer outside the NR. As shown in Fig. 1a, the Au NR seeds were prepared with a  $7.8 \pm 2.1$  nm width and a  $33.0 \pm 4.6$  nm length. Then, by reacting with different concentrations of  $\text{AgNO}_3$  in the growth solution, a series of Au@Ag nanoparticles (NPs) were synthesized and displayed different Ag layer thicknesses and shapes (Fig. 1b-e). When the  $\text{Ag}^+$  concentration was low (0.040 mM), a few Ag atoms were deposited and the Ag shell seemed to be more or less homogeneous over the entire NR. However, as the  $\text{Ag}^+$  concentration rose to 0.060 mM, the Ag nanolayer was obviously thickened and an anisotropic Ag coating occurred, although the resulted Au@Ag NPs remained in the rod shape with a  $9.6 \pm 2.3$  nm width and a  $32.8 \pm 4.4$  nm length. By further increasing the  $\text{Ag}^+$  concentration, the anisotropic degree was gradually

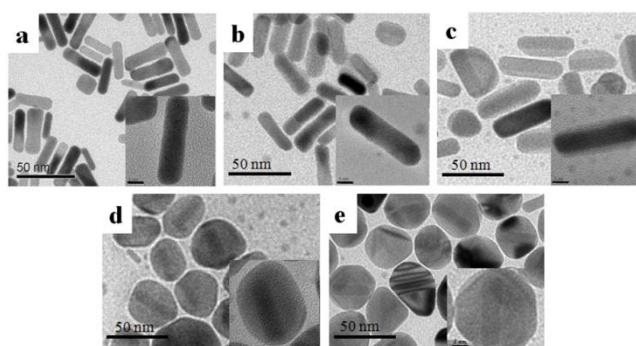


**Fig. 1** TEM images of (a) Au NRs and (b-e) Au@Ag NPs with different shapes prepared using different concentrations of  $\text{AgNO}_3$ . (b) 0.040 mM; (c) 0.060 mM; (d) 0.128 mM; (e) 0.384 mM. Scale bar: 50 nm. (Inserts: TEM images with higher magnification. Scale bar: 5 nm.)

enhanced. Particularly when the  $\text{Ag}^+$  concentration reached 0.384 mM, sphere-like Au@Ag NPs, which exhibited a clear differential contrast of the outside Ag layer from the inside darkened Au NR, were fabricated with a diameter of  $40.1 \pm 3.5$  nm. The corresponding absorption spectra investigation also showed that with the increase of Ag layer thickness, the longitudinal SPR band blue-shifted markedly, while the transverse SPR band slightly blue-shifted. These two bands were finally superposed and centered at  $\sim 400$  nm when sphere-like Au@Ag NPs formed (Fig. S1). It was indicated that by adjusting the concentration of  $\text{Ag}^+$  in the growth solution, a good morphological control of Au@Ag NPs could be facily achieved.

### 3.2 Synthesis and characterization of Au@Ag/Au NPs

In view of their weak absorbance in the NIR region and potential toxicity from Ag exposed to biological systems, Au@Ag NPs were then allowed to react with  $\text{HAuCl}_4$  to produce Au@Ag/Au NPs through transformation of the outside Ag into Ag/Au alloy. With the thickness increase of original Au@Ag NPs, the NIR absorbing intensity of Au@Ag/Au NPs exhibited a gradual enhancement (Fig. S2a). In particular, the Au@Ag/Au NPs prepared using Au@Ag nanospheres (NSs) (0.384 mM  $\text{AgNO}_3$ ) were endowed with a broad and intense absorption band from 400 to 1100 nm, which might be caused by the particle polydispersity in shape and size. And in the case of Au@Ag NSs reacting with different concentrations of  $\text{HAuCl}_4$ , it was found that the absorbance spectrum of Au@Ag/Au NPs would not change obviously unless the concentration of  $\text{HAuCl}_4$  was below  $68 \mu\text{M}$  (Fig. S2b).

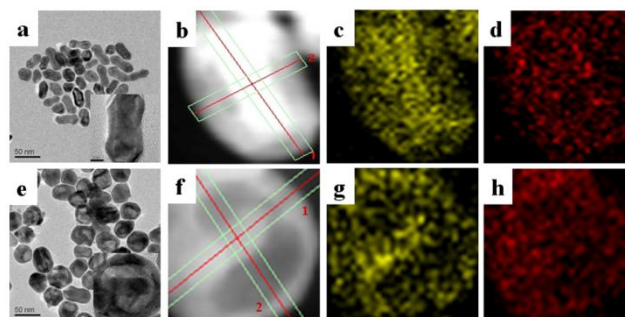


**Fig. 2** TEM images of (a) Au@Ag/Au NRs and (e) Au@Ag/Au NSs. Scale bar: 50 nm. (Inserts: TEM images with higher magnification. Scale bar: 5 nm.) (b-d) HAADF-STEM-EDS mapping results showing a single Au@Ag/Au NR image, the gold image (yellow) and the silver image (red). (f-h) HAADF-STEM-EDS mapping results showing a single Au@Ag/Au NS image, the gold image (yellow) and the silver image (red).

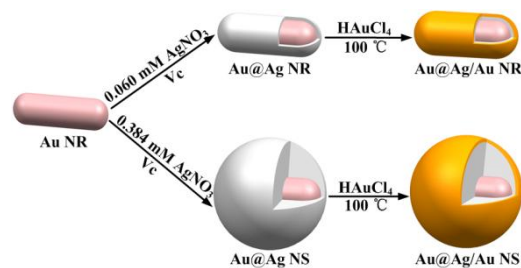


**Fig. 3** Schematic representation of the synthesis strategy of Au@Ag/Au NPs with different shapes.

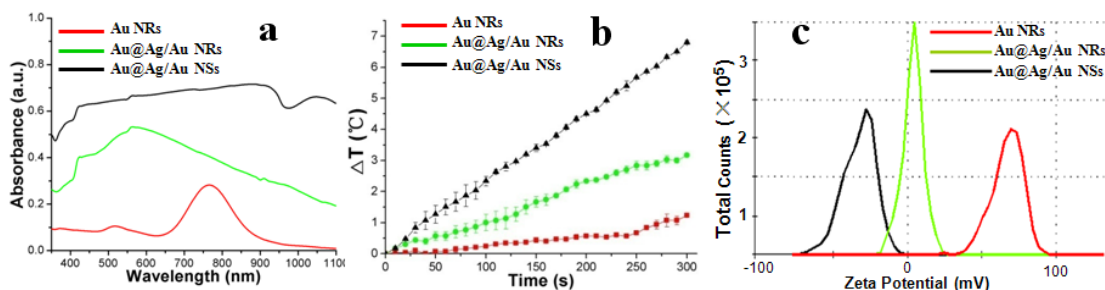


**Fig. 4** Property investigation of Au@Ag/Au NSs in comparison with Au NRs and Au@Ag/Au NRs. (a) UV-vis absorption spectra, all measured with  $2.2 \times 10^{10}$  particles/mL. (b) Heating curves using a 980 nm laser irradiation at 26.5 mW, all measured with  $4.4 \times 10^{10}$  particles/mL. (c) Zeta potential analysis, all measured with  $2.2 \times 10^{10}$  particles/mL.

Subsequently, two kinds of representative Au@Ag/Au NPs, including the one prepared using Au@Ag NRs (0.060 mM AgNO<sub>3</sub>) and the one prepared using Au@Ag NSs (0.384 mM AgNO<sub>3</sub>) were characterized by HRTEM and EDS. Results revealed that after the replacement reaction, the overall shapes and sizes of NPs were not changed significantly (Fig. 2a and 2e). But a core-shell structure with the Au NR core and the Ag/Au alloy shell was definitely observed for both Au@Ag/Au NRs (Fig. 2b-d) and Au@Ag/Au NSs (Fig. 2f-h) through EDS mapping analysis of a single NP. This was also confirmed by the line-scan EDS evaluation to measure their transverse and axial directions, which displayed the compositions of both Au and Ag, with a dominant Au in the middle part where the Au NR was located within the shell (Fig. S3).

Inspired by above investigation results, a shape-controllable and spectrum-adjustable synthesis strategy of Au@Ag/Au NPs could be outlined as shown in Fig. 3. Firstly, through the reaction of Au NR seeds with different concentrations of AgNO<sub>3</sub> in the growth solution, Au@Ag NPs with different shapes including rods, spheres, etc., could be fabricated. Next, through a replacement reaction with HAuCl<sub>4</sub>, the outside Ag/Au alloy could be formed<sup>32</sup> and thus endow Au@Ag/Au NPs with the greatly increased NIR absorbance and decreased toxicity. Due to the optical properties of Au@Ag/Au NPs were directly dependent upon their shapes, the adjustment of absorption spectra could be facilitated by controlling NPs' shapes according to practical needs.

### 3.3 Properties of Au@Ag/Au NSs

Concerning the application in biological systems, NIR absorption is a critical feature for ideal PTT agents. From this point of view, the as-prepared Au@Ag/Au NSs with a broad and strong absorption band from 400 to 1100 nm were deemed to be a promising PTT agent. Several properties of Au@Ag/Au NSs were then investigated by comparison with Au NRs and Au@Ag/Au NRs. As expected, at the same concentration, Au@Ag/Au NSs exhibited a much higher optical absorbing intensity than both Au NRs and Au@Ag/Au NRs (Fig. 4a). And the broad absorption band covering the visible and NIR region would promise a perfect adaptation to lasers with different wavelengths. Subsequently, a temperature elevation experiment was performed to test light-to-heat conversion efficiencies of these three NPs by using a 980 nm laser as the irradiation source. As shown in Fig. 4b, with the extension of exposure time, the temperature of Au@Ag/Au NSs solution achieved an increase of

$\sim 6.8$  °C in 5 min, in marked contrast to the small changes of the irradiated Au NRs (1.2 °C) and Au@Ag/Au NRs (3.1 °C). The hyperthermia effect of Au@Ag/Au NSs was estimated to be  $\sim 5.7$  times of Au NRs and  $\sim 2.2$  times of Au@Ag/Au NRs, respectively. Furthermore, the zeta potential analysis also revealed a gradual shift from  $53.5 \pm 10.1$  mV of Au NRs to  $3.78 \pm 7.06$  mV of Au@Ag/Au NRs and then to  $-32.2 \pm 10.9$  mV of Au@Ag/Au NSs at natural pH (Fig. 4c). It was speculated that during the process of Ag layer coating and Ag/Au shell formation, the toxic CTAB molecules with positive charges on Au NRs surface might be gradually removed or embedded. This would potentially bring a much lower dark-cytotoxicity to Au@Ag/Au

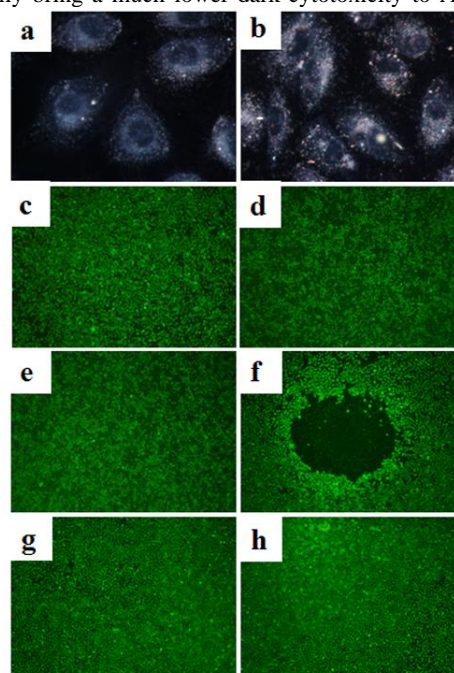


**Fig. 5** Feasibility investigation of Au@Ag/Au NSs for NIR PTT of cancer cells. (a, c, e) A549 cells without treatment by NPs; (b, d, f) A549 cells incubated with Au@Ag/Au NSs ( $2.2 \times 10^{10}$  particles/mL) for 6 h. (a, b) Dark-field images; (c, d) fluorescent images of cells without NIR irradiation; (e, f) fluorescent images of cells after NIR irradiation. (Green fluorescence indicates living cells.) A549 cells that incubated with (g) Au NRs ( $2.2 \times 10^{10}$  particles/mL) or (h) Au@Ag/Au NRs ( $2.2 \times 10^{10}$  particles/mL) for 6 h and then treated by NIR irradiation were also used as the control.

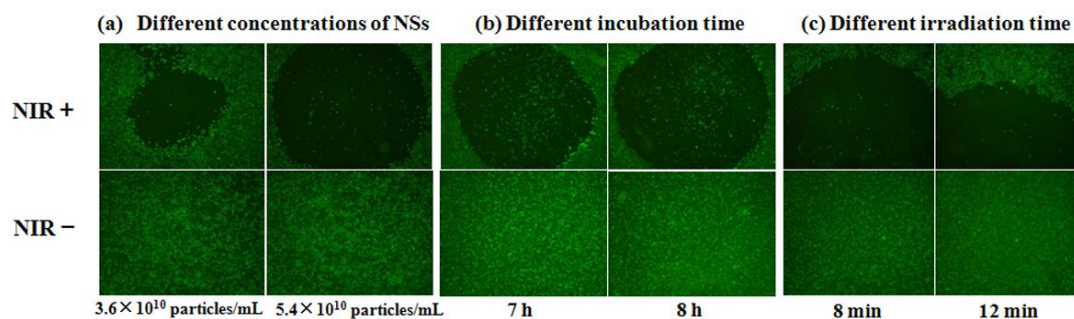


**Fig. 6** NIR PTT investigation of cancer cells with Au@Ag/Au NSs under different conditions. (a) A549 cells treated by different concentrations of Au@Ag/Au NSs for 6 h, (up) with or (bottom) without NIR irradiation for 5 min; (b) A549 cells treated by Au@Ag/Au NSs ( $2.2 \times 10^{10}$  particles/mL) for 5 different time, (up) with or (bottom) without NIR irradiation for 5 min; (c) A549 cells (up) with or (bottom) without treatment by Au@Ag/Au NSs ( $2.2 \times 10^{10}$  particles/mL) for 6 h, exposed to NIR irradiation for different time. (Green fluorescence indicates living cells.)

NSs. Thereupon, it is concluded that Au@Ag/Au NSs, which hold a broad, intense absorption and highly efficacious hyperthermia in the NIR window, are positively qualified optical heaters for PTT in biological systems.

### 3.4 NIR PTT of cancer cells using Au@Ag/Au NSs

In order to test the PTT efficacy of Au@Ag/Au NSs on biological samples, A549 lung adenocarcinoma cell line was selected as the main model. Through dark-field microscopy, the interaction of NSs with cells was firstly investigated (Fig. 5a and 5b). Results showed that a high density of bright pink spots indicating the presence of NSs were obviously observed on the cell surface or inside cells after incubation with NSs. While for cells without treatment, there were only light blue signals detected as a result of autofluorescence and scattered light from organelles. It was revealed that Au@Ag/Au NSs could effectively interact with A549 cells. Then, the NIR PTT of cancer cells was carried out by using calcein-AM, a non-fluorescent dye that could permeate cell membrane and be hydrolyzed by intracellular esterases to a green fluorescent calcein dye in live cells, to assess cell viability. As displayed in Fig. 5f, after exposure to a 980 nm laser at 26.5 mW for 5 min, the apparent cell death in the irradiation region was imaged for cells treated by NSs. In contrast, cells without any treatment (Fig. 5c), cells only incubated with NSs without irradiation (Fig. 5d) and cells only irradiated without incubation with NSs (Fig. 5e) all exhibited bright green fluorescence, implying no obvious cell death. It was indicated that Au@Ag/Au NSs could efficaciously achieve the NIR light-to-heat conversion to kill cancer cells. And no obvious dark-cytotoxicity was observed for Au@Ag/Au NSs, which was further proved by using a PI-based dead cell staining method to quantitatively test the cytotoxicity of Au@Ag/Au NSs (Fig. S4). In addition, a comparison with Au NRs (Fig. 5g) and Au@Ag/Au NRs (Fig. 5h) also showed that under the same condition, cells treated by these two NPs still preserved perfect viability, suggesting a much higher PTT efficacy of Au@Ag/Au NSs.

Whereafter, a systematic investigation of the influence of several factors, including NSs concentration, incubation time and irradiation time, on the PTT efficacy of Au@Ag/Au NSs was performed. As shown in Fig. 6a, by further increasing the concentration of NSs for cell treating, a gradual expansion of dead cell areas was detected. After incubation with  $5.4 \times 10^{10}$

particles/mL NSs for 6 h, a NIR irradiation for just 5 min destroyed most of the cells in the whole visual field. A similar phenomenon was also observed by extending the incubation time to 8 h (Fig. 6b). It was speculated that longer incubation time might lead to more NSs interacting with cells, thus producing stronger PTT effects. However, no matter the increased concentration of NSs or the extended incubation time did not visibly affect the viability of cells without exposure to NIR light. This confirmed the low dark-cytotoxicity of Au@Ag/Au NSs once again. Next, a better way to enhance PTT efficacies was found by prolonging the exposure time to NIR light. As presented in Fig. 6c, a NIR irradiation for up to 12 min was definitely safe for cells without treatment by NSs. While for cells incubated with  $2.2 \times 10^{10}$  particles/mL NSs for 6 h, the dead cell area was sharply broadened so that its radius went far beyond the visual field. It was implied that Au@Ag/Au NSs held a great potential for the NIR PTT of cancer. Thereupon, the adaptability of Au@Ag/Au

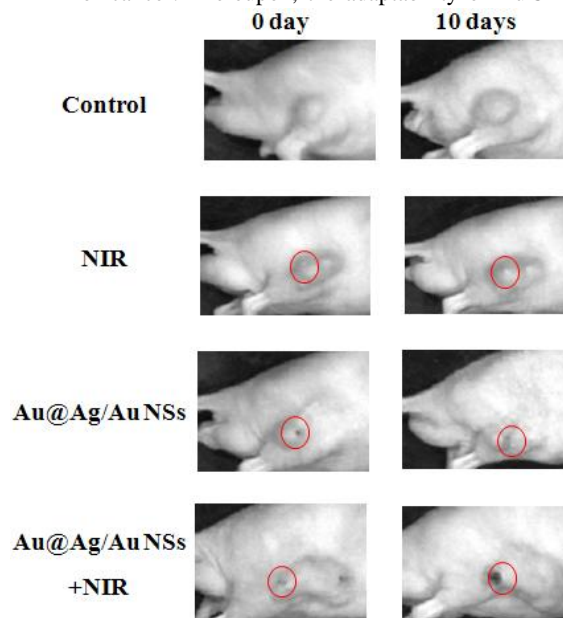


**Fig. 7** Feasibility investigation of Au@Ag/Au NSs for *in vivo* NIR PTT using A549 tumor-bearing mice as the model. The PTT effect was assessed by observing tumor necrosis. (The red circle indicates the injection site or irradiation region.)

NSs for the PTT of other cells was testified by using QBC-939 cholangiocarcinoma cells and SPCAI lung adenocarcinoma cells. Results indicated that after incubation with NSs, both kinds of cells could be effectively destructed under the NIR irradiation (Fig. S5).

### 3.5 *In vivo* NIR PTT using Au@Ag/Au NSs

A primary application of Au@Ag/Au NSs in the NIR PTT of cancer *in vivo* was then conducted by using A549 tumor-bearing mice as the model. Four groups of mice were investigated with different treating strategies, including one group without any treatment, one group with only NIR irradiation, one group with only NSs injection and one group with both NIR irradiation and NSs injection. The PTT efficacy was assessed by observing the tumor necrosis ten days after treatment. As shown in Fig. 7, only the tumor that received an injection of NSs and then irradiated by a 980 nm laser for 5 min exhibited an obvious necrosis. In contrast, ten days later, tumors in other three control groups still keep intact without any sign of cancer destruction. The result suggests that Au@Ag/Au NSs are a kind of promising PTT agents for *in vivo* cancer therapy.

## 4 Conclusions

In this paper, a novel, washing-free, shape-controllable and spectrum-adjustable synthesis strategy of Au@Ag/Au NPs was developed by firstly coating a Ag nanolayer outside the Au NR and then reacting with HAuCl<sub>4</sub> to yield a Ag/Au alloy nanoshell. The shape of NPs could be facily controlled by changing the concentration of AgNO<sub>3</sub> in the growth solution. The transformation of outside Ag into Ag/Au alloy could greatly enhance the NIR absorbance of NPs. The optimized Au@Ag/Au NSs held a broad and intense absorption band from 400 to 1100 nm, thus producing ~5.7 times hyperthermia effect of Au NRs and promising a perfect adaptation to laser sources with different wavelengths. Particularly, if a continuous NIR irradiation source is employed, their PTT effects might be further improved due to the extremely broad absorption cross section. *In vitro* investigation then demonstrated that Au@Ag/Au NSs could not only efficaciously destruct different kinds of cancer cells, but also hold low dark-cytotoxicity. A primary *in vivo* application also revealed that Au@Ag/Au NSs held a great potential for cancer therapy in real biological systems. As a promising NIR PTT agent, the specificity of Au@Ag/Au NSs would be improved by introducing cancer-targeted molecules, such as antibodies, aptamers, *etc.*<sup>33,34</sup> Moreover, due to Au@Ag/Au NSs simultaneously have signal output and therapy function, they might be potentially applied in theranostics.

## Acknowledgements

This work was supported in part by the National Natural Science Foundation of China (Grants 21175039, 21190044, 21221003, 21322509, 21305035 and 21305038), Research Fund for the Doctoral Program of Higher Education of China (Grant 20110161110016), the project supported by Hunan Provincial Natural Science Foundation and Hunan Provincial Science and Technology Plan of China (2012TT1003), and the Fundamental Research Funds for the Central Universities.

## Notes and references

- State Key Laboratory of Chemo/Biosensing and Chemometrics, College of Chemistry and Chemical Engineering, Institute of Biology, Hunan University, Key Laboratory for Bio-Nanotechnology and Molecular Engineering of Hunan Province, Changsha 410082, China. Fax: +86 731 88821566; Tel: +86 731 88821566; E-mail: kmwang@hnu.edu.cn.*  
 † Electronic Supplementary Information (ESI) available: [Figs. S1-S5]. See DOI: 10.1039/b000000x/  
 ‡ Joint first author.
- 1 S. Lal, S. E. Clare and N. J. Halas, *Acc. Chem. Res.*, 2008, **41**, 1842.
  - 2 X. H. Huang, P. K. Jain and I. H. El-Sayed, *Lasers Med. Sci.*, 2008, **3**, 17.
  - 3 S. Shibua, M. Hamadaa, N. Murasea and V. Biju, *J. Photoch. Photobio. C*, 2013, **15**, 53.
  - 4 V. Ntziachristos, J. Ripoll, L. V. Wang and R. Weissleder, *Nat. Biotechnol.*, 2005, **23**, 313.
  - 5 S. E. Skrabalak, J. Y. Chen, Y. G. Sun, X. M. Lu, L. Au, C. M. Copley and Y. N. Xia, *Acc. Chem. Res.*, 2008, **41**, 1587.
  - 6 A. F. Bagley, S. Hill, G. S. Rogers and S. N. Bhatia, *ACS Nano*, 2013, **7**, 8089.
  - 7 H. Y. Tang, S. Shen, J. Guo, B. S. Chang, X. G. Jiang and W. L. Yang, *J. Mater. Chem.*, 2012, **22**, 16095.
  - 8 X. H. Huang, I. H. El-Sayed, W. Qian and M. A. El-Sayed, *J. Am. Chem. Soc.*, 2006, **128**, 2115.
  - 9 L. Gao, J. Zhao, H. Li, Y. Cui and J. B. Li, *ACS Nano*, 2012, **6**, 8030.
  - 10 J. Y. Chen, D. L. Wang, J. F. Xi, L. Au, A. Siekkinen, A. Warsen, Z. Y. Li, H. Zhang, Y. N. Xia and X. L. Li, *Nano Lett.*, 2007, **7**, 1318.
  - 11 L. Cheng, K. Yang, Y. G. Li, J. H. Chen, C. Wang, M. W. Shao, S. T. Lee, and Z. Liu, *Angew. Chem. Int. Ed.*, 2011, **50**, 7385.
  - 12 H. T. Ke, J. R. Wang, Z. F. Dai, Y. S. Jin, E. Z. Qu, Z. W. Xing, C. X. Guo, X. L. Yue and J. B. Liu, *Angew. Chem. Int. Ed.*, 2011, **123**, 3073.
  - 13 J. T. Robinson, S. M. Tabakman, Y. Y. Liang, H. L. Wang, H. S. Casalongue, D. Vinh and H. J. Dai, *J. Am. Chem. Soc.*, 2011, **133**, 6825.
  - 14 Y. W. Wang, Y. Y. Fu, Q. L. Peng, S. S. Guo, G. Liu, J. Li, H. H. Yang and G. N. Chen, *J. Mater. Chem. B*, 2013, **1**, 5762.
  - 15 A. L. Antaris, J. T. Robinson, O. K. Yaghi, G. S. Hong, S. Diao, R. Luong and H. J. Dai, *ACS Nano*, 2013, **7**, 3644.
  - 16 L. Wang, J. J. Shi, H. L. Zhang, H. X. Li, Y. Gao, Z. Z. Wang, H. H. Wang, L. L. Li, C. F. Zhang, C. Q. Chen, Z. Z. Zhang and Y. Zhang, *Biomaterials*, 2013, **34**, 262.
  - 17 L. C. Cheng, J. H. Huang, H. M. Chen, T. C. Lai, K. Y. Yang, R. S. Liu, M. Hsiao, C. H. Chen, L. J. Her and D. P. Tsa, *J. Mater. Chem.*, 2012, **22**, 2244.
  - 18 C. L. Chen, L. R. Kuo, S. Y. Lee, Y. K. Hwu, S. W. Chou, C. C. Chen, F. H. Chang, K. H. Lin, D. H. Tsai and Y. Y. Chen, *Biomaterials*, 2013, **34**, 1128.
  - 19 N. R. Jana, *Small*, 2005, **1**, 875.
  - 20 D. W. Wang, X. M. Zhu, S. F. Lee, H. M. Chan, H. W. Li, S. K. Kong, J. C. Yu, C. H. K. Cheng, Y. X. J. Wang and K. C.-F. Leung, *J. Mater. Chem. B*, 2013, **1**, 2934.
  - 21 G. Maltzahn, A. Centrone, J. H. Park, R. K. Ramanathan, M. J. Sailor, T. A. Hatton and S. N. Bhatia, *Adv. Mater.*, 2009, **21**, 3175.
  - 22 S. Pandey, M. Thakur, A. Mewada, D. Anjarlekar, N. Mishra and M. Sharon, *J. Mater. Chem. B*, 2013, **1**, 4972.
  - 23 W. I. Choi, J. Y. Kim, C. Kang, C. C. Byeon, Y. H. Kim and G. Tae, *ACS Nano*, 2011, **5**, 1995.
  - 24 H. T. Ke, J. R. Wang, Z. F. Dai, Y. S. Jin, E. Z. Qu, Z. W. Xing, C. X. Guo, J. B. Liu and X. L. Yue, *J. Mater. Chem.*, 2011, **21**, 5561.
  - 25 Z. M. Li, P. Huang, X. J. Zhang, J. Lin, S. Yang, B. Liu, F. Gao, P. Xi, Q. S. Ren and D. X. Cui, *Mol. Pharm.*, 2009, **7**, 94.
  - 26 C. H. Wang, C. W. Chang and C. A. Peng, *J. Nanopart. Res.*, 2011, **13**, 2749.
  - 27 P. K. Jain, X. H. Huang, I. H. El-sayed and M. A. El-sayed, *Acc. Chem. Res.*, 2008, **41**, 1578.
  - 28 J. L. Li, D. Day and M. Gu, *Adv. Mater.*, 2008, **20**, 3866.
  - 29 J. H. Park, G. Maltzahn, L. L. Ong, A. Centrone, T. A. Hatton, E. Ruoslahti, S. N. Bhatia and M. J. Sailor, *Adv. Mater.*, 2010, **22**, 880.

- 
- 30 K. W. Hu, T. M. Liu, K. Y. Chung, K. S. Huang, C. T. Hsieh, C. K. Sun and C. S. Yeh, *J. Am. Chem. Soc.*, 2009, **131**, 14186.
- 31 M. F. Tsai, S. H. G. Chang, F. Y. Cheng, V. Shanmugam, Y. S. Cheng, C. H. Su and C. S. Yeh, *ACS Nano*, 2013, **7**, 5330.
- 5 32 W. Xiong, D. Sikdar, M. Walsh, K. J. Si, Y. Tang, Y. Chen, R. Mazid, M. Weyland, I. D. Rukhlenko, J. Etheridge, M. Premaratne, X. Y. Li and W. L. Cheng, *Chem. Commun.*, 2013, **49**, 9630.
- 33 B. V. Broek, A. D. Hollander, H. L. Gijs, K. Jans, L. Lagae, S. Muyldermans, G. Maes and G. Borghs, *ACS Nano*, 2011, **5**, 4319.
- 10 34 W. T. Lu, A. K. Singh, S. A. Khan, D. Senapati, H. T. Yu and P. C. Ray, *J. Am. Chem. Soc.*, 2010, **132**, 18103.